Effect of spin-orbit interactions on the structural stability, thermodynamic properties, and transport properties of lead under pressure

N. A. Smirnov*

Russian Federal Nuclear Center - Institute of Technical Physics, 456770, Snezhinsk, Russia

(Received 5 February 2018; published 28 March 2018)

The paper investigates the role of spin-orbit interaction in the prediction of structural stability, lattice dynamics, elasticity, thermodynamic and transport properties (electrical resistivity and thermal conductivity) of lead under pressure with the FP-LMTO (full-potential linear-muffin-tin orbital) method for the first-principles band structure calculations. Our calculations were carried out for three polymorphous lead modifications (fcc, hcp, and bcc) in generalized gradient approximation with the exchange-correlation functional PBEsol. They suggest that compared to the scalar-relativistic calculation, the account for the SO effects insignificantly influences the compressibility of Pb. At the same time, in the calculation of phonon spectra and transport properties, the role of SO interaction is important, at least, for $P \lesssim 150$ GPa. At higher pressures, the contribution from SO interaction reduces but not vanishes. As for the relative structural stability, our studies show that SO effects influence weakly the pressure of the fcc $\rightarrow$ hcp transition and much higher the pressure of the hcp $\rightarrow$ bcc transition.

DOI: 10.1103/PhysRevB.97.094114

I. INTRODUCTION

Nowadays one can find a good many papers devoted to the investigation of the effect of spin-orbit (SO) interaction on the properties of pure metals calculated from first-principles (see, for example, Refs. [1–18] and references in them). The authors use different methods for calculation and different approaches for the description of exchange-correlation interaction (various LDA and GGA XC functionals). They more often focus on the ground-state properties such as the equilibrium specific volume V_0 and bulk modulus B_0. However, the SO effect can weakly manifest itself in these properties and much stronger in others, e.g., the phonon spectrum or relative stability of different structures both under ambient and under elevated pressure [13,18]. Material compression markedly changes interaction between particles in the system and might also change the contribution of SO effects to the system energy. It is worth noting that calculations that account for SO coupling are about an order of magnitude more time consuming than the scalar-relativistic ones. The ability to avoid more costly calculations without a noticeable loss of accuracy is often very necessary in determining the properties of matter.

Lead is one of the interesting metals where the effect of SO interaction manifests itself [16–19]. Under ambient conditions it has a simple face-centered cubic structure. Experimental data on phonon spectra dispersion for noncompressed lead show some anomalies [20,21]. As demonstrated in different DFT calculations, only relativistic calculations that account for SO coupling are capable of reproducing these anomalies with good accuracy [16–19]. As a result, it becomes possible to more accurately determine the electron-phonon and transport spectral distribution functions, the electron-phonon coupling strength, and some other quantities [18,19,22]. The *ab initio* calculations reported in Refs. [16–19] are done with pseudopotential methods both in local (LDA) [16,18,19] and in nonlocal (GGA) [17] approximation for the exchange-correlation functional. It should be noted here that the phonon frequencies calculated with and without SO coupling may differ by tens of percents [16], while the SO effect on the ground-state properties of lead, V_0 and B_0, is insignificant [15–19].

Lead was also actively investigated under pressure in static experiments. Experimental data from x-ray analysis show that Pb under pressure undergoes two structural transitions, fcc $\rightarrow$ hcp and hcp $\rightarrow$ bcc, at pressures $P \approx 13 \pm 1$ and $\approx$109 GPa, respectively [23–27]. Further compression up to 272 GPa did not show any structural changes [24,26]. *Ab initio* calculations for the relative stability of fcc, hcp, and bcc lead by the pseudopotential approach (LDA calculations) with SO interaction were done in Ref. [28] and gave rather good agreement with experiment. Though the authors of Ref. [28] note the effect of SO interaction on the relative stability of different Pb structures, it is not clear how exactly it influences the pressures of the structural transitions. This issue is earlier considered in more detail in Ref. [29] where calculations are done by the LMTO method in the tight-binding approximation (LMTO-TB). The authors [29] state that firstly, the absence of relativistic effects incorrectly reproduces the equilibrium crystal structure (diamond instead of fcc), and secondly, allowance for SO interaction makes agreement between experimental and calculated pressures of the fcc $\rightarrow$ hcp transition much better compared to the ordinary scalar-relativistic calculations.

The boundaries of structural transitions under increasing pressure and temperature were investigated in static experiments where lead was compressed in a laser-heated diamond anvil cell [27,30]. In Ref. [27], the behavior of the fcc-hcp phase boundary was investigated in the temperature range from room to $T \approx 800$ K. In this range, the boundary was shown to run almost vertically in the PT diagram, i.e., the

*deldavis@mail.ru

pressure of the fcc → hcp transition was nearly unchanged with increasing temperature. The authors of Ref. [30] obtained the boundary of hcp and bcc coexistence in the PT diagram of lead at temperatures above 1800 K. The line has a negative slope and a triple point hcp-bcc-liquid at $P \approx 39$ GPa and $T \approx 2400$ K. They also measured the melting curve of lead to 80 GPa. Currently, there are no *ab initio* calculations that would provide information on the stability boundaries of different structures of compressed lead at $T > 0$ and the effect of SO interaction on them.

This paper aims to investigate the effect of SO interaction on the calculation of some thermodynamic, elastic, and transport properties of lead, as well as its relative structural and dynamic stability at pressures from zero to hundreds of gigapascal. *Ab initio* calculations with and without SO coupling are compared with different experimental results and, in special cases, with nonrelativistic calculations to see the role of relativity in the *ab initio* calculations of various properties of Pb. Three experimentally observed structures, specifically fcc, hcp, and bcc, are investigated. Unlike most papers where lead properties are calculated with the pseudopotential methods, the results reported in this paper are obtained with the all-electron full-potential method.

II. CALCULATION METHOD

Lead properties are calculated with the well-known FP-LMTO (full-potential linear-muffin-tin orbital) method of band structure calculation, implemented in the LMTART package [31,32]. The $5d$, $6s$, and $6p$ electrons of Pb are taken to be valence electrons; semicore electrons are not considered. The equilibrium value for the parameter c/a of the hcp phase is determined by minimizing the dependence of crystal specific energy, $E_{\text{tot}}(c/a)$, for each of the compressions considered. The temperature dependence of c/a is neglected.

The wave functions of core electrons are determined by solving the Dirac equation with the spherically symmetric part of crystal potential. For valence electrons, the relativistic effects are considered approximately. The scalar-relativistic Hamiltonian includes the mass-velocity and Darwin corrections. Spin-orbit interaction is treated as a perturbation with the corresponding term in the Hamiltonian in the form of energy-dependent operator [32–34].

The internal parameters of the method were adjusted so as to ensure acceptable accuracy in the calculation of specific energy E_{tot} (about 0.1 mRy/atom). For this purpose we investigated how the values of E_{tot} depended on the parameters. Integration over the Brillouin zone was done with an improved tetrahedron method [35]. The **k**-point grid was taken to be $24 \times 24 \times 24$ for the cubic structures and $24 \times 24 \times 12$ for the hexagonal one. These grids are quite sufficient for predicting thermodynamic properties with acceptable accuracy, but the calculation of the electron-phonon (EP) interaction matrix requires finer meshes [36]. Therefore we used $32 \times 32 \times 32$ (fcc, bcc) and $36 \times 36 \times 18$ (hcp) grids for the EP matrix calculations. The cutoff energy for representing basis functions as a plane-wave expansion in the interstitial region depended on the degree of crystal compression, but always was no lower than 680 eV. The basis set included MT orbitals with moments $l^b_{\max} = 3$ The spherical harmonic expansion of charge density and potential was done to the moment $l^w_{\max} = 7$ The values of such FP-LMTO parameters as linearization energies, tail energies, and MT-sphere radius R_{MT} were chosen similarly to the approach described in Ref. [12], i.e., so as to minimize the internal energy of the crystal. The optimal value of R_{MT} is equal to 3.17 a.u. The phonon spectra were calculated from linear response theory implemented in the FP-LMTO code [31]. In the case of the cubic structures, phonon frequencies ω_j were obtained on grids of $8 \times 8 \times 8$ **q** points. For the hexagonal one, it was $8 \times 8 \times 6$. The contribution of lattice vibrations to free energy was determined in a quasiharmonic approximation [37] with the use of the calculated phonon spectra. The elastic constants of fcc, hcp, and bcc structures were calculated with an approach, which is described in detail in Refs. [38,39]. The method is based on the calculation of specific energy as a function of crystal deformation at arbitrary isotropic pressure.

The GGA exchange-correlation functional PBEsol [40] is used for calculations. As shown in Refs. [15,41], it reproduces the ground-state properties and compression isotherm of lead most accurately compared to other GGA and LDA functionals. Our calculations also show PBEsol to be best fit to the description of lead behavior under pressure. So, if we compare the equilibrium specific volumes V_0 calculated with the PBEsol and PBE [42] functionals, the disagreement with experiment is more than 6% for PBE and less than 1% for PBEsol. The latter also describes the bulk modulus of lead much better [41].

The transport properties, specifically electrical resistivity ρ and thermal conductivity w^{-1}, are calculated within the lowest-order variational approximation LOVA described in Ref. [43]. LOVA is based on an approximated solution of the Boltzmann equation under the condition that the Fermi distribution is rigidly shifted by the applied electrical field. Phonon drag and thermoelectric effects are neglected in this approximation. Expressions for ρ and w^{-1} at the specific volume V are defined by [36,43]

$$\rho(Tx) = \frac{\pi V k_B T}{N(E_F)\langle v_x^2\rangle} \int_0^\infty \frac{d\omega}{\omega} \frac{x^2}{\sinh^2 x} \alpha^2_{\text{tr}} F(\omega), \quad (1)$$

$$w(T) = \frac{6V}{\pi k_B N(E_F)\langle v_x^2\rangle} \int_0^\infty \frac{d\omega}{\omega} \frac{x^2}{\sinh^2 x} \cdot \left[\alpha^2_{\text{tr}} F(\omega) + \frac{4x^2}{\pi^2}\alpha^2_{\text{out}} F(\omega) + \frac{2x^2}{\pi^2}\alpha^2_{\text{in}} F(\omega)\right]. \quad (2)$$

Here, $x = \omega/(2k_BT)$, $N(E_F)$ is the electron density of states on the Fermi level, $\langle v_x^2\rangle$ is the average square of the x component of the Fermi velocity, and $\alpha^2_{\text{tr}} F(\omega) = [\alpha^2_{\text{out}} F(\omega) - \alpha^2_{\text{in}} F(\omega)]$ is the transport spectral function (for more detail see Refs. [36,43]). All the quantities required for the determination of electrical resistivity and thermal conductivity from expressions 1 and 2 can be calculated by the FP-LMTO method, as it is shown in Ref. [36].

III. CALCULATION RESULTS

A. Phonon spectrum

See first how the phonon spectrum of lead changes with the different degree of account for the relativistic effects. Figure 1 shows a part of the phonon spectrum in the Γ-K-X direction of the Brillouin zone and the phonon density of states (PDOS)

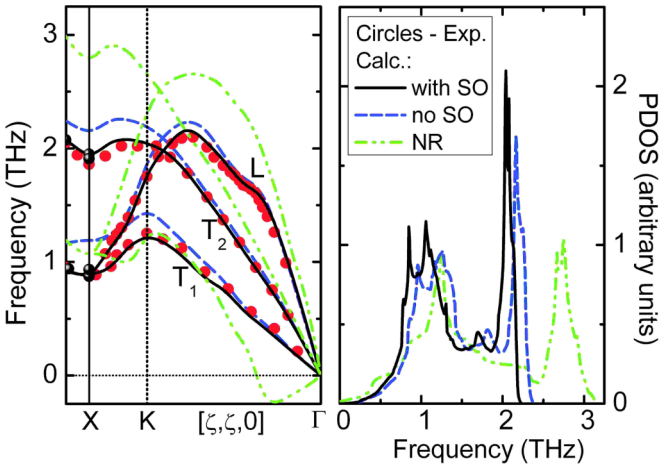

FIG. 1. (Left) Phonon frequencies of fcc Pb at $T = 0$ K in the Γ-K-X direction of the Brillouin zone from calculations with different degrees of account for the relativistic effects (NR: nonrelativistic). Red and black circles show experimental results [20,44] at $T = 100$ K. (Right) Phonon density of states of fcc Pb for the specified variants of calculation. Both the pictures are for $V/V_0 = 1$.

of fcc Pb for three variants of calculation at $V/V_0 = 1$ ($V_0 = 200.14$ a.u.^{3} is the experimental specific volume at $T = 0$ K [15]). These are results of nonrelativistic (NR) calculations and relativistic calculations without (no SO) and with SO coupling.

It is seen from Fig. 1 (left panel) that the fcc structure is dynamically unstable when the relativistic effects are absent. The acoustic phonon branch T_1 near the Γ point becomes negative. It should be noted that our NR calculations show the fcc phase to remain dynamically unstable even for compressed lead. Also, there is in fact no anomaly in the longitudinal phonon branch in the interval Γ-K, and maximal frequencies are about 1.5 times higher than experimental values. As seen from Fig. 1, partial account for relativity (no SO) dynamically stabilizes fcc lead and gives much better agreement with experiment. The above mentioned anomaly now appears in the longitudinal vibrational branch in the Γ-K interval. But phonon branches are somewhere still noticeably higher than the experimental values. Accounting for SO interaction again improves the situation and gives the best agreement with experiment. If we now neglect a small part of the NR spectrum with negative frequencies and look at the phonon density of states (Fig. 1, right panel), we will see that our step-by-step inclusion of the relativistic effects shifts the phonon spectrum to lower frequencies.

Let us consider how the phonon dispersion changes as pressure increases. A special feature of fcc Pb is the presence of a well noticed dip in the spectrum of phonon frequencies near the X point of the Brillouin zone, both in the longitudinal and transverse vibrational branches [20,21]. Figure 2 shows phonon frequencies in the Γ-X-W direction at different values of relative specific volume from calculations of two types. As stated above, account for the SO effects markedly improves agreement between calculation and experiment (Fig. 2, upper panel), especially at point X. Results obtained in the present work agree well with the earlier pseudopotential calculations from Refs. [16–18]. Our calculations show that with increasing

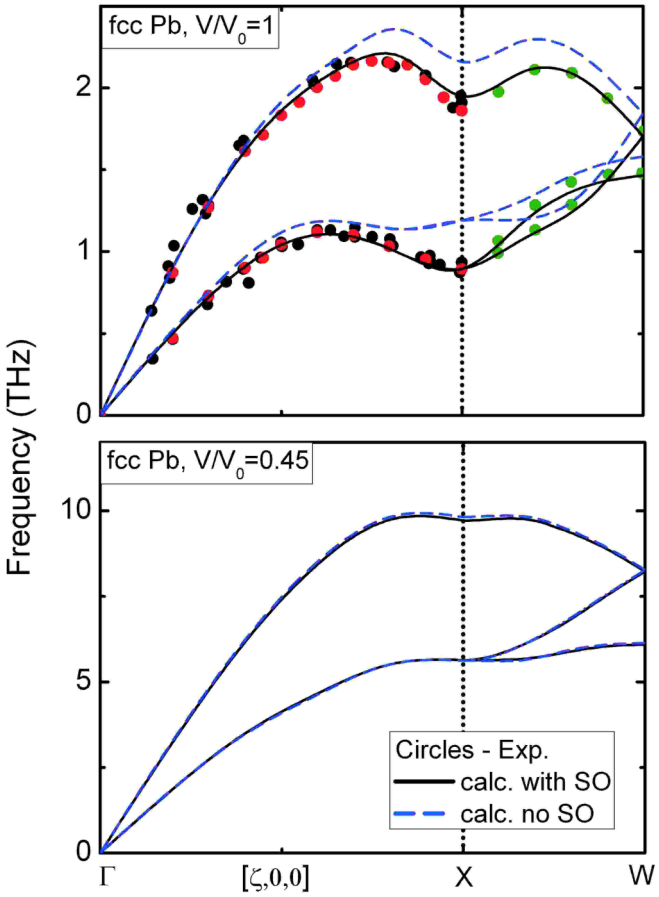

FIG. 2. Phonon frequencies of fcc Pb at two values of V/V_0 in Γ-X-W direction of the Brillouin zone from our calculations with and without SO effects. The red and black dots show experimental data from [20,44] at $T = 100$ K, and the green ones show data from [21] at $T = 80$ K.

pressure, first, the dips near point X disappear in both branches of the phonon spectrum, and second, results with and without SO coupling become almost identical (Fig. 2, lower panel).

Now consider how the phonon spectrum of lead changes, on whole, with increasing compression. Figure 3 shows the phonon density of states (PDOS) of fcc Pb for two compressions and two variants of calculation. It is seen (Fig. 3, upper panel) that at $V/V_0 = 1$, PDOS calculated with SO effects agrees with experiment much better than that obtained without SO coupling. Differences in the phonon densities of states from two types of calculation reduce as pressure increases and becomes almost indistinguishable (Fig. 3, lower panel). That is, high pressure gradually cancels the SO effect on the calculated phonon spectra. This tendency is seen for all considered structures. In order to quantitatively demonstrate how compression changes the differences in the results of two types of calculation, we evaluated the contribution of lattice vibrations to the free energy of the system in a quasiharmonic approximation. Figure 4 shows the difference $\Delta F^{\rm ph} = (F^{\rm ph}_{\rm noSO} - F^{\rm ph}_{\rm SO})$ of thermal contributions to the free energy at $T = 300$ K from calculations with and without SO effects for fcc, hcp, and bcc lead. For all the three phases, $\Delta F^{\rm ph}$ is seen to decrease with the decreasing relative specific volume. At $V/V_0 < 0.625$, it

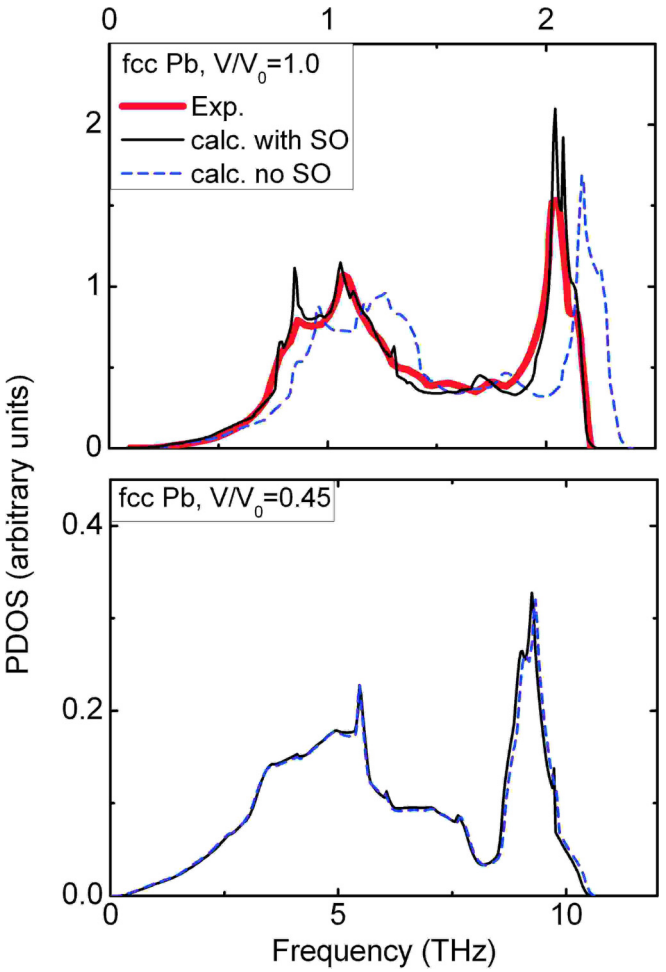

FIG. 3. Phonon density of states of fcc Pb for two values of the relative specific volume V/V_0. Our calculations with and without SO coupling (black and blue lines) are compared with experiment Ref. [21] at $T = 80$ K (red line).

becomes smaller than the specified calculation accuracy of E_{tot} (0.1 mRy/atom). It should be noted here that at $T = 0$ K, bcc Pb is dynamically unstable in both variants of calculation if $V/V_0 > 0.7$. Moreover, in calculations with SO, the bcc phase remains dynamically unstable to a bit higher compressions.

In order to comment on the above changes, let us consider the evolution of the band structure of Pb crystal under compression. Figure 5 shows the electron densities of states (DOS) for fcc lead from our calculations at $V/V_0 = 1.0$ and 0.45 with and without SO coupling. At normal specific volume, the spectrum of valence electrons is seen as a set of bands jointed in a number of separated "stripes" (Fig. 5, upper panel). As seen from the figure, there is the splitting of $5d$ zones due to the SO interaction. There are also noticeable differences in the density of states of $6p$ electrons. With increasing pressure, the "stripes" gradually join together. At first, it takes place at $V/V_0 \approx 0.75$ with the $6p$ and $6s$ bands and then, at $V/V_0 \approx 0.65$–0.475, the $6p$-$6s$ "stripe" joins the $5d$ bands (Fig. 5, lower panel). In the process, the differences in the densities of states near the Fermi level obtained in calculations with and without SO coupling gradually decrease. This is seen if we compare the DOS on E_F (N_F) in two variants of calculation shown in the

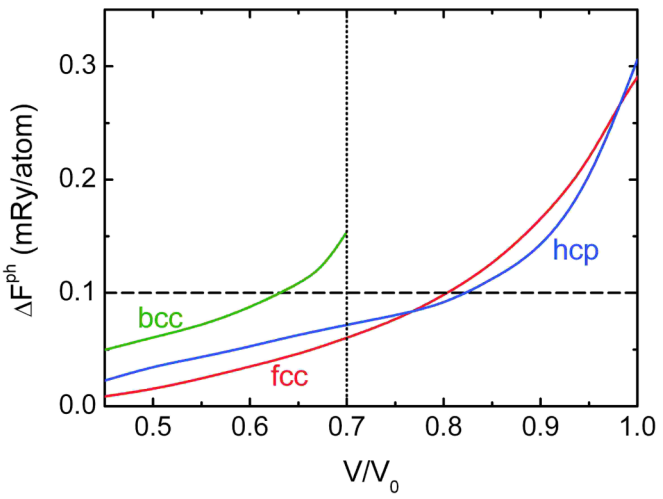

FIG. 4. The difference of thermal contributions to the free energy at $T = 300$ K from lattice vibrations, obtained in calculations without and with SO effects for the three considered structures. The vertical dotted line shows the boundary of bcc dynamical stability.

inset of Fig. 5 (upper panel). The difference in N_F, which is well seen when compressions are small, becomes vanishing at $V/V_0 < 0.6$, and the results with SO effects gradually approach those without SO coupling as the specific volume decreases. The applied external pressure changes interaction in the system and smoothes peculiarities in the electron DOS so that the effect from the SO interaction becomes insignificant, at least for some of the physical quantities. Nevertheless, as it will be shown later, there are other quantities where the influence of SO effects is not negligible even at high pressures.

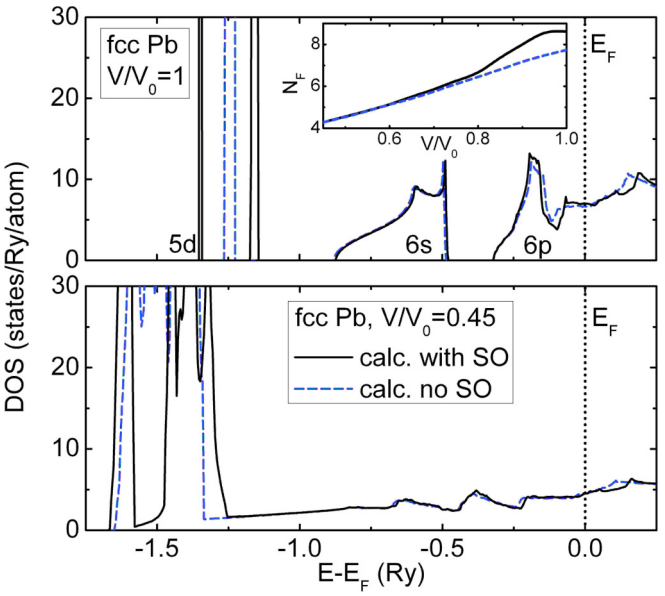

FIG. 5. Electron density of states for fcc Pb at different compressions and $T = 0$ K for two types of calculation. For convenience, the figures are cut along the axis of ordinates. The inset in the upper panel shows electron densities of states on the Fermi level for different values of V/V_0.

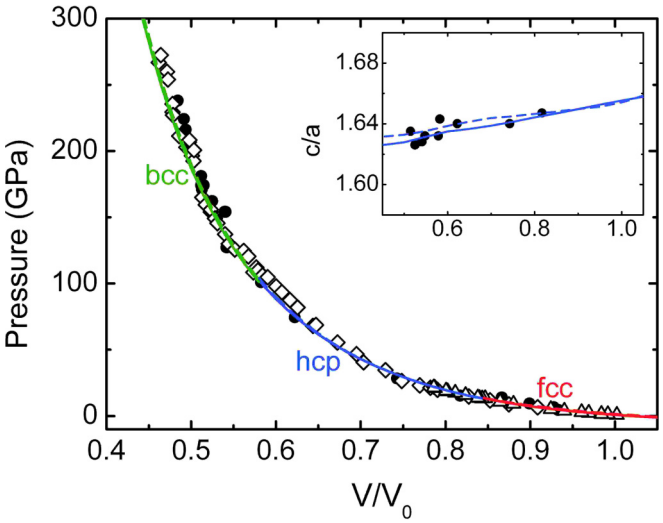

FIG. 6. Compression curves at room temperature for three lead structures in comparison with experiment. Solid lines show calculations with SO, the dashed lines are calculations without SO effects. Experiment: • [24], ◇ [26], and △ [27]. The inset shows c/a vs V/V_0 for hcp Pb in comparison with experiment [24].

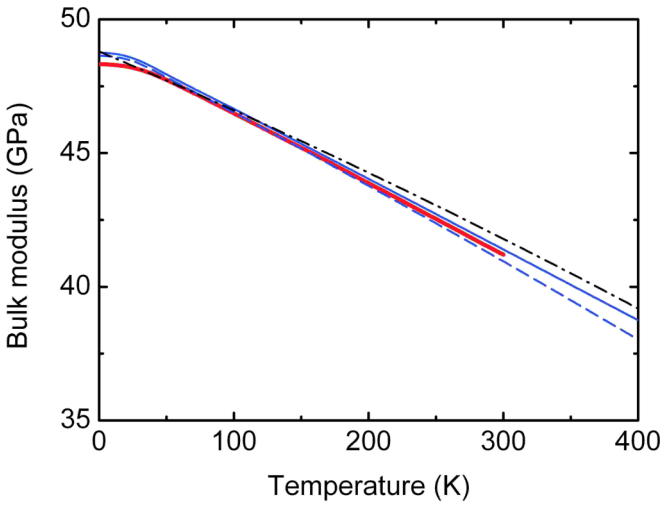

FIG. 7. Bulk modulus vs temperature for fcc Pb in comparison with experiment. The solid blue line shows the calculation with SO, and the dashed one shows calculation without SO interaction. The red line shows experimental data [15], and the dash-dotted one shows data obtained from the experimental EOS [45].

B. Compression curves, elasticity, and relative structural stability

Let us next turn to SO effects on the compression curves determined at room temperature, and on the temperature dependence of bulk modulus. Figure 6 shows the isotherms 300 K calculated for fcc, hcp, and bcc lead with account for structural transformations, in comparison with experiment. Results from two types of calculation are seen to run very closely and agree well with experiment. The equilibrium specific volume at room temperature equals 204.3 a.u.^{3} with SO and 206.8 a.u.^{3} without SO coupling, and its experimental value is 204.8 a.u.^{3} [15]. So, the error of its determination is less than 1% in both cases. The inset in Fig. 6 also compares the dependence of c/a for hcp Pb with experimental data. One can see a small difference between the results of two calculations and good agreement with experiment.

Figure 7 presents the temperature dependencies of isotermal bulk modulus B_0 calculated for fcc lead in the quasiharmonic approximation. It also shows data obtained in a recent experiment [15] and results of the equation of state (EOS) [45], which are based on earlier experimental data. At room temperature, B_0 equals 41.4 GPa in calculations with SO and 40.9 GPa in calculations without SO interaction, the experimental value is $B_0 = 41.2$ GPa [15]. The calculated dependencies $B_0(T)$ agree well with experiment and results obtained with the EOS of Ref. [45]. Spin-orbit coupling influences $B_0(T)$ rather weakly; at $T = 400$ K, the values obtained in the two calculations differ by no more than about 2%. So, it can be stated that the contribution of spin-orbit effects to compression curves and the temperature dependence of B_0 is quite small.

The effect of SO interaction on elastic constants is a bit higher. At $V/V_0 = 1$ and $T = 0$ K, calculations with SO coupling give the following constants for fcc Pb: $C' = 5.59$ and $C_{44} = 19.98$ GPa [$C' = (C_{11} - C_{12})/2$], while calculations without SO effects give $C' = 5.75$ and $C_{44} = 22.25$ GPa. The difference makes up 3% and 11% for C' and C_{44}, respectively. The experimental values reported in Ref. [46] are $C' = 5.06$ and $C_{44} = 19.42$ GPa. Calculations with SO coupling are seen to agree better with experimental results. The difference between two types of calculations gradually disappears as pressure increases. Table I shows the elastic constants fcc, hcp, and bcc structures of lead with account for the SO effects. As stated above, bcc Pb is dynamically unstable at $V/V_0 > 0.7$

TABLE I. Elastic constants (in GPa) of three lead structures at different specific volumes and $T = 0$ K (calculations with SO coupling).

V/V_0	C_{11}	C_{12}	C_{13}	C_{33}	C_{44}
		fcc structure			
1.00	54.51	43.33	–	–	19.98
0.95	71.73	58.22	–	–	25.17
0.90	93.03	77.17	–	–	31.98
0.85	119.8	101.3	–	–	40.25
0.80	151.6	131.0	–	–	51.15
		hcp structure			
0.90	112.5	75.93	56.47	121.9	30.48
0.85	145.2	102.2	74.91	153.6	38.39
0.75	232.1	172.4	124.6	246.8	61.70
0.65	367.6	292.4	212.7	425.5	106.4
0.60	478.5	394.4	288.5	572.3	143.1
0.55	655.2	557.6	396.9	746.7	186.7
		bcc structure			
0.675	252.2	243.3	–	–	110.0
0.65	295.3	278.6	–	–	124.2
0.60	407.4	373.0	–	–	161.3
0.55	569.7	509.3	–	–	218.2
0.50	808.1	714.6	–	–	294.7
0.45	1176.1	1034.6	–	–	430.2

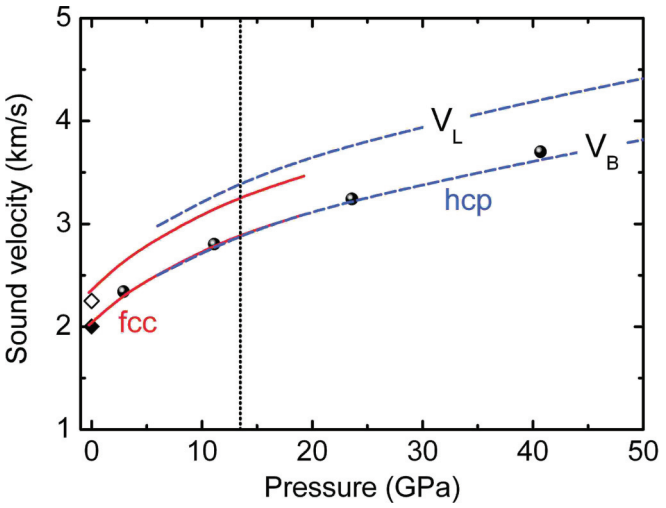

FIG. 8. Longitudinal and bulk sound velocities vs pressure for polycrystalline Pb. Our calculation with SO effects: solid red lines are for fcc, blue dashed lines are for hcp. Experiments: ♢, ♦ Ref. [47], ● Ref. [48]. The dotted vertical line shows the approximate boundary of the fcc → hcp transition.

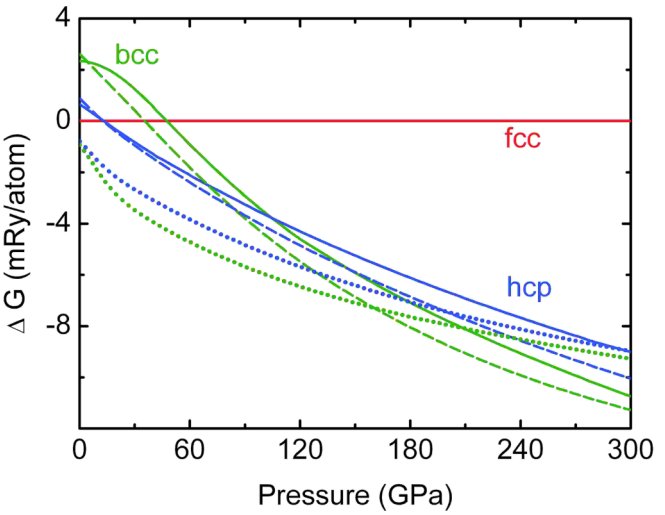

FIG. 9. Gibbs potential differences of fcc, hcp, and bcc Pb vs pressure at $T = 0$ K (without zero-point vibrations). The solid lines show calculations with SO, the dashed ones show calculations without SO coupling, and the dotted lines show nonrelativistic calculations (NR).

and $T = 0$ K, which is confirmed by the calculated elastic constants. An instability appears in the tetragonal deformation of the lattice ($C' < 0$).

With the elastic constants for single crystal Pb, we can calculate the pressure dependencies of the longitudinal and bulk sound velocities for polycrystalline lead by Voigt-Reuss-Hill averaging [49]. Figure 8 presents results for fcc and hcp lead versus available experimental data [47,48]. Calculation and experiment are seen to agree rather well. The vertical line in Fig. 8 shows the approximate boundary of the fcc → hcp transition. It can be seen that the bulk sound velocity is practically free of drastic changes during the transition, while the longitudinal one has a small discontinuity of about 4%.

Now we focus on the relative structural stability of lead under pressure. Figure 9 shows the Gibbs potential differences from three types of calculations (relativistic with and without SO effects, and nonrelativistic) for the considered crystal structures at $T = 0$ K up to 300 GPa. As noted in Ref. [29], in the absence of relativistic effects, the equilibrium crystal structure of lead is reproduced incorrectly. It is seen from Fig. 9 that bcc Pb has the lowest energy at $P = 0$ in NR calculations. With the increasing pressure it remains the most energetically favorable up to $P = 300$ GPa, at least. Also, the hcp phase is more favorable than the fcc one. In the relativistic treatment, the pattern changes drastically (Fig. 9) the transitions occur in the correct order, fcc → hcp → bcc both with SO and without SO coupling. Table II contains transition pressures P_{tr} from two types of our calculations (with SO and no SO) along with experimental results. Note that the account for SO effects weakly changes the pressure of the fcc → hcp transition; its value is almost the same for both variants of calculations and well agrees with experiment. That is, FP-LMTO calculations with SO coupling do not show a strong change of the pressure of the fcc → hcp transition, unlike the LMTO-TB calculations [29] where P_{tr} shifts by about 10 GPa. However, the values of P_{tr} obtained with and without SO interaction for the hcp → bcc transition differ markedly (by about 20%). With account for SO effects, the agreement between calculation and experiment becomes much better (see Table II). In order to see how the calculated results on the relative structural stability of Pb depend on the type of the XC functional, we did additional calculations with the Gunnarsson-Lundqvist functional [50], with gradient corrections [51], which quite well reproduced the properties of lead in its ground state. These calculations confirm what was earlier stated for the PBEsol functional (see Table II). The different type of XC functionals only slightly shifts the values of P_{tr}.

With the calculated internal energies and phonon spectra of fcc, hcp, and bcc Pb, we determined the phase boundaries in the quasiharmonic approximation for nonzero temperatures. Figure 10 shows the PT diagram of lead up to 150 GPa. Here, the melting curve is taken from the experiment of Ref. [30]. It is seen from Fig. 10 that the fcc-hcp phase boundaries obtained with and without SO coupling are almost identical and agree well with the experimental line from Ref. [27]. The slight reduction of the transition pressure at $T > 800$ K

TABLE II. Transition pressures P_{tr} from two types of calculation ($T = 0$ K) in comparison with experiment at room temperature. The value of P_{tr} from Ref. [30] is the value from Ref. [25] corrected according to the pressure scale [52]. XC GL denotes our calculations with functional [50] and gradient corrections [51].

		P_{tr} (GPa)	
	Type of calc.	fcc → hcp	hcp → bcc
Calc.	XC PBEsol, no SO	12.8	85
	XC PBEsol, with SO	13.2	104.5
	XC GL, no SO	16.6	89.4
	XC GL, with SO	16.1	117.2
Exp.	–	13 ± 1 [23]	109 [25],104 [30]

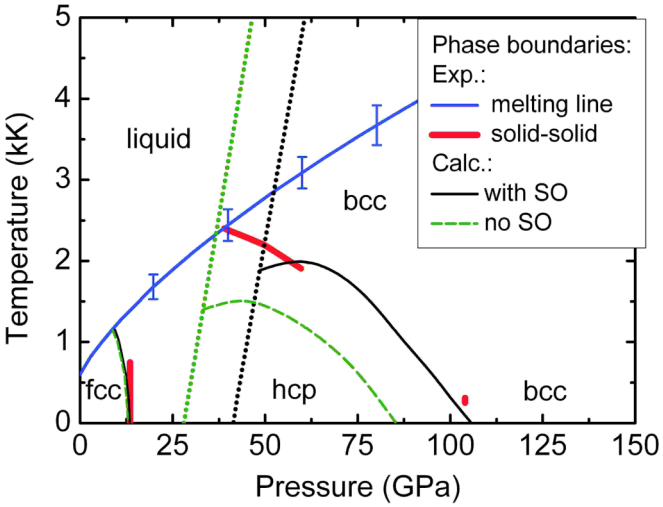

FIG. 10. PT diagram of lead. The solid black lines show phase boundaries from our calculation with SO, and the dashed green ones are the boundaries from the calculation without SO coupling. The blue line shows the experimental melting curve [30]; the red lines are fcc-hcp and hcp-bcc phase boundaries determined in experiments [27,30]. The dotted lines are the boundaries of the dynamical stability of bcc Pb from the calculation with (black) and without (green) SO effects. To the left of these lines the bcc structure is dynamically unstable.

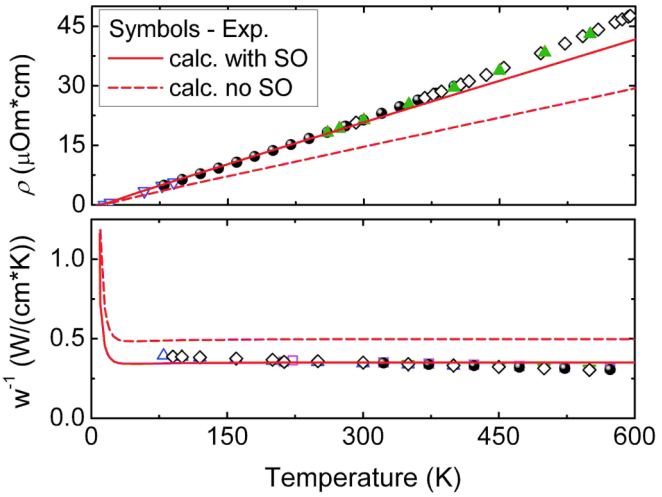

FIG. 11. Electrical resistivity (top) and thermal conductivity (bottom) of fcc Pb at $V/V_0 = 1$ from calculations with (solid lines) and without (dashed lines) SO interaction. Symbols show the experimental results [55,56].

might be caused by the insufficiently accurate calculation of anharmonic effects in the quasiharmonic approximation (no phonon-phonon interaction). It is, however, not improbable that such a decrease in pressure will be observed in experiment at temperatures higher than 800 K. Here, we must note that the contribution of anharmonic effects to the system energy can be neutralized by the thermal excitation of electrons as it was shown in Ref. [53].

The situation with the hcp-bcc phase boundary is more complicated (see Fig. 10). As mentioned earlier, the bcc structure is dynamically unstable at relatively low compressions ($V/V_0 > 0.7$). As a result, the PT diagram has a pressure range where it is impossible to determine the quasiharmonic contribution from the nuclei thermal vibrations to the energy of the system. Here, we have to more accurately consider the anharmonic effects because they can dynamically stabilize the bcc phase at high temperatures, as it happens, for example, in titanium, zirconium, or hafnium [54]. But in our paper, the consideration is limited to the quasiharmonic approximation. Therefore the dotted lines in Fig. 10 show the boundary of the dynamical stability of bcc Pb for calculations with and without SO coupling. This boundary differs in the calculations with SO and no SO because the values of V/V_0 at which the structure becomes dynamically unstable are slightly different. It is seen from Fig. 10 that the hcp-bcc phase boundaries from two types of calculation have a very close slope but markedly differ in pressure. At temperatures above 1400 K and $P < 60$ GPa, both the curves change the sign of slope because the phonon spectrum of the bcc structure softens near the region of its dynamic instability. On the whole, the hcp-bcc boundary from the calculation with SO coupling is seen to agree much better with experiment than the boundary obtained without SO interaction. However, its correct determination at $T > 1500$ K requires a step beyond the limit of quasiharmonic approximation since the additional contribution from vibrational entropy in this temperature range can crucially change the calculated results [54].

C. Electrical resistivity and thermal conductivity

Consider how the transport properties of lead depend on temperature and the degree of crystal compression. Figure 11 compares the temperature dependencies of electrical resistivity and thermal conductivity for fcc Pb at $V/V_0 = 1$ from two types of calculation and from several experiments. With the SO effects, both are seen to be much more accurate. The effect of SO coupling on ρ and w^{-1} is the highest of all the physical quantities considered. In the temperature range $100 \lesssim T \lesssim 300$ where LOVA calculations are most accurate [43], the difference between two types of calculation makes up about 30% for ρ and 40% for w^{-1}. The same results for electrical resistivity obtained recently with the pseudopotential approach are reported in Ref. [19].

Let us see how the pattern changes when compression increases. Begin with Fig. 12, which shows resistivity ρ versus pressure at room temperature up to $P = 100$ GPa with account for the fcc → hcp structural transition. The electrical resistivity is seen to strongly reduce as pressure increases. The curves $\rho(P)$ calculated with and without SO coupling are seen to gradually approach each other because the increasing compression reduces differences in the phonon spectra and the densities of states on the Fermi level from two types of calculation. On the boundary of the fcc → hcp transition, $\rho(P)$ has a characteristic discontinuous rise. The inset in Fig. 12 compares the calculated relative electrical resistivity with the available experimental data [57,58] in the vicinity of the structural transition. One can see that calculations without SO effects noticeably underestimate resistivity and the magnitude of $\rho/\rho_0(P)$ jumps in the pressure-induced phase transition. The situation greatly improves when SO interaction is included. A

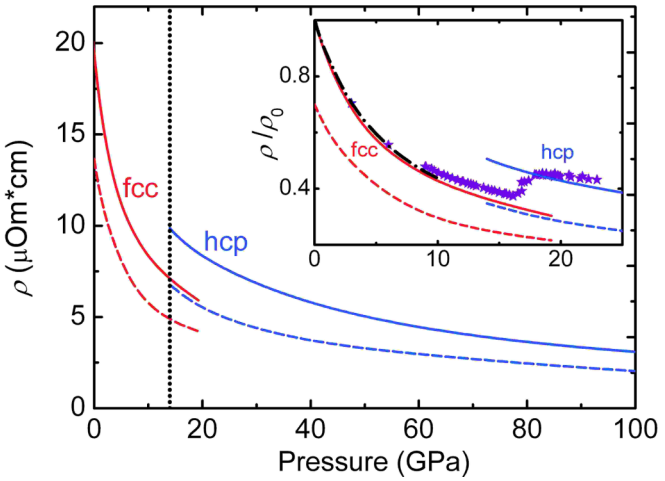

FIG. 12. Electrical resistivity vs pressure for fcc and hcp Pb at room temperature from calculations with (solid lines) and without (dashed lines) SO effects. The vertical dotted line shows the experimental pressure of fcc → hcp transition [23]. The inset shows the $\rho/\rho_0(P)$ dependencies with stars for experimental data [57] and the dash-dotted line for the approximation of experiment [58]. ρ_0 is the resistivity at $P = 0$ and $T = 300$ K.

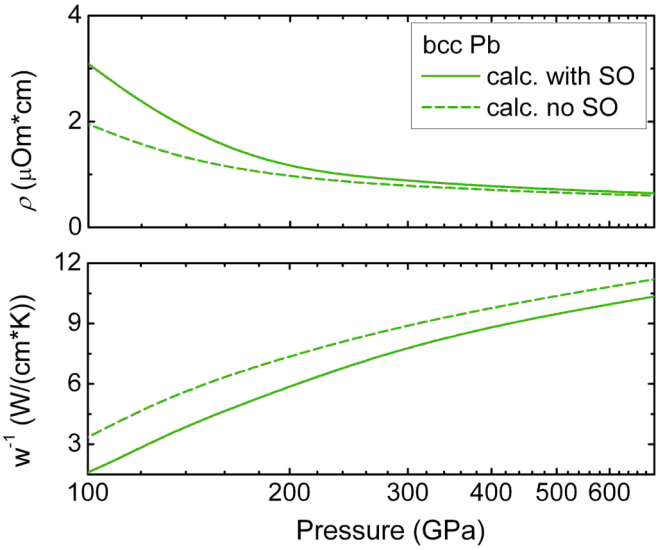

FIG. 13. Electrical resistivity (upper panel) and thermal conductivity (lower panel) vs pressure for bcc lead at room temperature from calculations with (solid lines) and without (dashed lines) SO effects.

small discrepancy between SO calculations and experimental results at $P > 5$ GPa can be caused, on the one hand, by the error, which appears due to insufficient calculation accuracy. The accuracy of our determination of ρ under pressure relative to the method parameters is estimated to be about 10%. On the other hand, in experiment [57], the pressure in the region of the structural transition was determined through the extrapolation of Bridgman data on lead isothermal compression to 3 GPa. By data from Ref. [57], the resistivity jumps at 16.1 GPa, that is, a bit higher than the value of P_{tr} determined in the x-ray diffraction analysis of paper [23] (13 ± 1 GPa). A better agreement is reached with data from the more recent experiment reported in Ref. [58].

At pressures higher than 100 GPa, bcc lead is most thermodynamically favorable. Therefore we consider just this structure for $P > 100$ GPa. Figure 13 presents the values of ρ and w^{-1}, which were computed for two types of calculation. The results obtained with and without SO effects are seen to approach as pressure increases. At $P = 700$ GPa, they differ by no more than about 8%, while under ambient conditions the difference exceeds 30%. The remaining difference at such high pressures is mainly due to the velocity $\langle v_x^2 \rangle$ present in formulas 1 and 2. This velocity is determined by averaging the band energy derivative with respect to wave vector $\mathbf{k}$, $v_{n\mathbf{k}} = \partial\varepsilon_{n\mathbf{k}}/\partial\mathbf{k}$, and hence directly depends on the width of the corresponding band. As our calculations show, despite that the electron densities of states near E_F from calculations with and without SO coupling get closer, the bandwidths somewhat differ and give the above difference by 8%. The tendency seen in Fig. 13 suggests that the difference will go on to reduce with increasing compression.

IV. CONCLUSIONS

We have discussed the role of spin-orbit interaction in the FP-LMTO calculations of lead properties in a wide range of pressures. Our studies show that the degree of its influence on different properties markedly differs. The inclusion of SO effects always makes the calculated results better, i.e., closer to experimental data. Under ambient conditions, SO interaction has the greatest effect on the transport properties of lead. Their calculations with and without SO coupling may differ by 30% and more. Such a discrepancy is mainly caused by differences in the phonon spectra from the two types of calculation. With increasing pressure, the discrepancy significantly decreases and the effect of SO interaction gradually weakens. At $P \approx 700$ GPa, the differences are no greater than 8%. SO interaction has the smallest effect on the isotherms and bulk modulus of lead ($\lesssim$2%). A bit higher effect, about 10%, is seen for elastic constants at $P = 0$, but it also reduces as crystal compression grows.

The effect of SO interaction manifests itself differently in the determination of structural stability of Pb under pressure. So, it is weak (about 3%) for the calculated pressure of the fcc → hcp transition, and rather strong (about 20%) for that of the hcp → bcc transition. Our studies have clearly demonstrated that taking the correct account of anharmonicity (phonon-phonon interaction) requires that the hcp-bcc boundary at $T > 1500$ K should be determined more accurately than it is done in the usual quasiharmonic approximation we used here. Our calculations show bcc lead to be dynamically unstable at $V/V_0 > 0.7$ ($P < 45$ GPa) and $T = 0$ K. Phonon mode softening leads to losses in the accuracy of free energy calculation and eventually to difficulties in the determination of the hcp-bcc boundary at high temperatures and moderate pressures.

[1] P. H. T. Philipsen and E. J. Baerends, Phys. Rev. B **61**, 1773 (2000).

[2] V. Theileis and H. Bross, Phys. Rev. B **62**, 13338 (2000).

[3] M. D. Jones, J. C. Boettger, R. C. Albers, and D. J. Singh, Phys. Rev. B **61**, 4644 (2000).
[4] L. Nordström, J. M. Wills, P. H. Andersson, P. Söderlind, and O. Eriksson, Phys. Rev. B **63**, 035103 (2000).
[5] J. C. Boettger, Phys. Rev. B **64**, 035103 (2001).
[6] P. Söderlind, Phys. Rev. B **66**, 085113 (2002).
[7] N. Richard, S. Bernard, F. Jollet, and M. Torrent, Phys. Rev. B **66**, 235112 (2002).
[8] A. Dal Corso and A. Mosca Conte, Phys. Rev. B **71**, 115106 (2005).
[9] L. E. Díaz-Sánchez, A. H. Romero, M. Cardona, R. K. Kremer, and X. Gonze, Phys. Rev. Lett. **99**, 165504 (2007).
[10] L. W. Nixon, D. A. Papaconstantopoulos, and M. J. Mehl, Phys. Rev. B **78**, 214510 (2008).
[11] W. Xie, W. Xiong, C. A. Marianetti, and D. Morgan, Phys. Rev. B **88**, 235128 (2013).
[12] N. A. Smirnov, J. Phys.: Condens. Matter **29**, 105402 (2017).
[13] K. Kotmool, S. Chakraborty, T. Bovornratanaraks, and R. Ahuja, Sci. Rep. **7**, 42983 (2017).
[14] A. Hermann, J. Furthmüller, H. W. Gäggeler, and P. Schwerdtfeger, Phys. Rev. B **82**, 155116 (2010).
[15] T. Strässle, S. Klotz, K. Kunc, V. Pomjakushin, and J. S. White, Phys. Rev. B **90**, 014101 (2014).
[16] A. D. Corso, J. Phys.: Condens. Matter **20**, 445202 (2008).
[17] M. J. Verstraete, M. Torrent, F. Jollet, G. Zerah, and X. Gonze, Phys. Rev. B **78**, 045119 (2008).
[18] R. Heid, K.-P. Bohnen, I. Y. Sklyadneva, and E. V. Chulkov, Phys. Rev. B **81**, 174527 (2010).
[19] S. Poncé, E. Margine, C. Verdi, and F. Giustino, Comput. Phys. Comm. **209**, 116 (2016).
[20] B. N. Brockhouse, T. Arase, G. Cagliotti, K. R. Rao, and A. D. B. Woods, Phys. Rev. **128**, 1099 (1962).
[21] R. Stedman, L. Almqvist, and G. Nilsson, Phys. Rev. **162**, 549 (1967).
[22] I. Y. Sklyadneva, R. Heid, P. M. Echenique, K.-B. Bohnen, and E. V. Chulkov, Phys. Rev. B **85**, 155115 (2012).
[23] T. Takahashi, H. K. Mao, and W. A. Bassett, Science **165**, 1352 (1969).
[24] H. K. Mao, Y. Wu, J. F. Shu, J. Z. Hu, R. J. Hemley, and D. E. Cox, Solid State Commun. **74**, 1027 (1990).
[25] C. A. Vanderborgh, Y. K. Vohra, H. Xia, and A. L. Ruoff, Phys. Rev. B **41**, 7338 (1990).
[26] Y. K. Vohra and A. L. Ruoff, Phys. Rev. B **42**, 8651 (1990).
[27] A. Kuznetsov, V. Dimitriev, L. Dubrovinsky, V. Prakapenka, and H.-P. Weber, Solid State Commun. **122**, 125 (2002).
[28] A. Y. Liu, A. Garcia, M. L. Cohen, B. K. Godwal, and R. Jeanloz, Phys. Rev. B **43**, 1795 (1991).
[29] N. E. Christensen, S. Satpathy, and Z. Pawlowska, Phys. Rev. B **34**, 5977 (1986).
[30] A. Dewaele, M. Mezouar, N. Guignot, and P. Loubeyre, Phys. Rev. B **76**, 144106 (2007).
[31] S. Y. Savrasov, Phys. Rev. B **54**, 16470 (1996).
[32] http://physics.ucdavis.edu/savrasov/, see LMTART documentation.
[33] D. D. Koelling and B. N. Harmon, J. Phys. C: Solid State Phys. **10**, 3107 (1977).
[34] G. Kotliar, S. Y. Savrasov, K. Haule, V. S. Oudovenko, O. Parcollet, and C. A. Marianetti, Rev. Mod. Phys. **78**, 865 (2006).
[35] P. E. Blöchl, O. Jepsen, and O. K. Andersen, Phys. Rev. B **49**, 16223 (1994).
[36] S. Y. Savrasov and D. Y. Savrasov, Phys. Rev. B **54**, 16487 (1996).
[37] D. C. Wallace, *Thermodynamics of Crystals* (Wiley, New York, 1972).
[38] G. V. Sin'ko and N. A. Smirnov, J. Phys.: Condens. Matter **14**, 6989 (2002).
[39] G. V. Sin'ko, Phys. Rev. B **77**, 104118 (2008).
[40] J. P. Perdew, A. Ruzsinszky, G. I. Csonka, O. A. Vydrov, G. E. Scuseria, L. A. Constantin, X. Zhou, and K. Burke, Phys. Rev. Lett. **100**, 136406 (2008).
[41] G. I. Csonka, J. P. Perdew, A. Ruzsinszky, P. H. T. Philipsen, S. Lebègue, J. Paier, O. A. Vydrov, and J. G. Ángyán, Phys. Rev. B **79**, 155107 (2009).
[42] J. P. Perdew, K. Burke, and M. Ernzerhof, Phys. Rev. Lett. **77**, 3865 (1996); **78**, 1396(E) (1997).
[43] F. J. Pinski, P. B. Allen, and W. H. Butler, Phys. Rev. B **23**, 5080 (1981).
[44] B. N. Brockhouse, R. Arose, G. Cagliotti, M. Sakamoto, R. N. Sinclair, and A. D. B. Woods, *Inelastic Scattering Neutrons Solids Liquids* (IAEA, Vienna, 1961), p. 531.
[45] A. D. Fortes, I. G. Wood, M. Alfredsson, L. Vočadlo, K. S. Knight, W. G. Marshall, M. G. Tucker, and F. Fernandez-Alonso, High Press. Res. **27**, 201 (2007).
[46] D. L. Waldorf and G. A. Alers, J. Appl. Phys. **33**, 3266 (1962).
[47] Edited by S. P. Marsh, *Los Alamos Shock Hugoniot Data* (University of California Press, Berkeley, CA, 1980).
[48] L. V. Al'tshuler, S. B. Kormer, M. I. Brazhnik, L. A. Vladimirov, M. P. Speranskaya, and A. I. Funtikov, ZhETF **38**, 1061 (1960) [JETP **11**, 766 (1960)].
[49] R. Hill, Proc. Phys. Soc. London A **65**, 349 (1952).
[50] O. Gunnarsson and B. I. Lundqvist, Phys. Rev. B **13**, 4274 (1976).
[51] J. P. Perdew, J. A. Chevary, S. H. Vosko, K. A. Jackson, M. R. Pederson, D. J. Singh, and C. Fiolhais, Phys. Rev. B **46**, 6671 (1992); **48**, 4978(E) (1993).
[52] A. Dewaele, P. Loubeyre, and M. Mezouar, Phys. Rev. B **70**, 094112 (2004).
[53] A. Glensk, B. Grabowski, T. Hickel, and J. Neugebauer, Phys. Rev. Lett. **114**, 195901 (2015).
[54] P. Souvatzis, O. Eriksson, M. I. Katsnelson, and S. P. Rudin, Phys. Rev. Lett. **100**, 095901 (2008).
[55] J. Bass and K. H. Fischer, *Metals: Electronic Transport Phenomena*, edited by K.-H. Hellwege and J. L. Olsen, Landolt-Börnstein, New Series, Group III, Vol. 15, Pt. a (Springer-Verlag, Berlin, 1982).
[56] P. G. Klemens, G. Neuer, B. Sundqvist, C. Uher, and G. K. White, *Metals: Electronic Transport Phenomena*, edited by O. Madelung and G. White, Landolt-Börnstein, New Series, Group III, Vol. 15, Pt. c (Springer-Verlag, Berlin, 1991).
[57] A. S. Balchan and H. G. Drickamer, Rev. Sci. Instrum. **32**, 308 (1961).
[58] A. Eiling and J. S. Schilling, J. Phys. F: Metal Phys. **11**, 623 (1981).